Connell, K. J., Larson, M., and Kraus, N. C. 2007. Morphologic Modeling of Multiple Barrier Island Breaches for Regional Application. *Proceedings Coastal Sediments '07 Conference*, ASCE Press, Reston, VA, 2011-2073.

MORPHOLOGIC MODELING OF MULTIPLE BARRIER ISLAND BREACHES FOR REGIONAL APPLICATION

Kenneth J. Connell[1], Magnus Larson[2], Nicholas C. Kraus [1]

1. U.S. Army Engineer Research and Development Center, Coastal and Hydraulics Laboratory, 3909 Halls Ferry Road, Vicksburg, MS 39180-6199, USA. Kenneth.J.Connell@erdc.usace.army.mil; Nicholas.C.Kraus@erdc.usace.army.mil.
2. Department of Water Resources Engineering, Lund University, Box 118, S-221 00 Lund, Sweden. Magnus.Larson@tvrl.lth.se.

Abstract: This paper introduces a time-dependent model of regional barrier island breaching for multiple openings, whether as permanent inlets or as new breaches to the same bay. The model allows an arbitrary number of breaches and is forced by tide, storm surge, and wave set up. Limitations on the hydrodynamics, hence calculated breach evolution, are those associated with the Keulegan inlet model. The model includes possible closure or limited breaching by shoaling of the breach channel by longshore transport. Capabilities of the multiple breaching model are examined through eight sensitivity tests.

INTRODUCTION

A breach in a barrier island occurs if inundation with strong flow develops a channel through the barrier. The inundation may be forced from the ocean side or the bay side. During a breach, the initial channel typically expands vertically and horizontally in exponential manner (Kraus 2003) to dynamic equilibrium dimensions. Forcing of the water flow in the breach is caused by a difference between bay and ocean water levels, influenced by wave runup and overwash.

High ocean water surface elevations and large waves associated with severe storms can produce multiple breaches along a coastal barrier island complex at regional spatial scales. Occurrences of multiple breach channels cut by storms has been reported (e.g., Price 1947; Terchunian and Merkert 1995; Wamsley and Hathaway 2004; Wutkowski 2004; Freeman et al. 2004), but there remains a paucity of quantitative barrier island

breach field data. Reviews of coastal barrier island breaching causes, processes, and remediation are given by Kraus and Wamsley (2003) and Wamsley and Kraus (2005).

Kraus and Hayashi (2005) developed a process-based numerical model to simulate morphologic evolution of coastal barrier island breaching for engineering use. The objective of the present study is to extend the capabilities of the Kraus and Hayashi model to include development and evolution of multiple breaches in areas along a barrier island, which may include presence of permanent inlets. This multiple-breach morphological model is applied on regional spatial scales by integration with the Cascade model of regional sediment transport and shoreline change (Larson et al. 2002; Larson and Kraus 2003; Larson et al. 2006; Connell and Kraus 2006; Larson et al. 2007).

COASTAL BREACH MODEL

The morphologic breaching model is based on analytical models for inlet stability and inlet channel cross-sectional area (Kraus 1998, 2003), and it has been extended to include morphologic evolution of a rectangular barrier island (Kraus 2003) and a stacked rectangle pyramidal barrier island (Kraus and Hayashi 2005). Studies have examined predictions of the coastal breach morphology model by comparison to field and laboratory breaches (Kraus and Hayashi 2005; Wamsley et al. 2006; Wamsley et al. 2007). The coastal breaching model simulates breaching by iteratively solving the 1-D Keulegan (1967) equations for inlet hydrodynamics to determine breach current velocity and bay elevation through time based on breach channel cross-sectional area and area of the bay. The coastal breaching model calculates under the assumptions that the bay must accommodate uniform water surface deviation, the bay is composed of vertical walls so that volume and surface area are directly correlated, and the breaches do not overlap.

If multiple breach channels are calculated to occur in the simulation, the Keulegan equations become:

$$\frac{\partial U_i}{\partial t} + \frac{g}{L_i}\left(\eta_B - \eta_O\right) + \left(K_{en,i} + K_{ex,i} + \frac{2c_{f,i}L_i}{R_{h,i}} \right)\frac{|U_i|U_i}{2L_i} = 0 \qquad (1)$$

for momentum, and:

$$\sum_{i=1}^{N} (A_c)_i U_i = A_{Bay}\frac{d\eta_B}{dt} \qquad (2)$$

for conservation of water volume, where U_i = depth-averaged and inlet-length integrated current velocity at breach or inlet i of N openings; t = time; g = gravitational acceleration; L = width of breach through the barrier island; η_O = water surface deviations from Mean Sea Level (MSL) in the ocean; K_{en} and K_{ex} = entrance and exit losses, respectively (non-dimensional); R_H = hydraulic radius of the breach or inlet (m); A_C = breach or inlet channel cross-sectional area below MSL (m^2); A_{Bay} = surface area of the bay (m^2). The bottom friction coefficient c_f is represented by Mannings formula,

$$c_f = gn^2 / h^{1/3} \qquad (3)$$

in which n = Mannings coefficient typically set as 0.025 s/m$^{1/3}$; and h = water depth.

Sediment transport through the breach is calculated employing the Watanabe et al. (1991) total load formula:

$$q_B = \alpha \frac{(\tau_m - \tau_c)}{\rho g} U \tag{4}$$

in which α = empirical coefficient typically of order 0.1 to 10 (non-dimensional); $\tau_m = c_f \rho \langle |U| U \rangle$, the time-averaged bottom shear stress for waves and current; $\tau_c = (\rho_s - \rho) g d_{50} \Psi_C$, the critical shear for sediment motion, where ρ_s is the density of sand (kg/m^3), ρ is the density of water (kg/m^3), d_{50} = median grain size diameter (m); and Ψ_C = critical Shields parameter, set to 0.05 for fine to medium sand.

If waves are not included in the breaching simulation, Eq. 4 becomes:

$$q_B = \alpha \left[\frac{n^2}{h^{1/3}} U^3 - \left(\frac{\rho_S}{\rho} - 1 \right) d_{50} \Psi_C U \right] \tag{5}$$

Sediment transport along the walls of the channel is calculated as a fraction of the transport along the breach floor. A typical value for side transport is approximately 70% of the transport along the channel.

$$q_S = \beta q_B \tag{6}$$

where β is the calibration factor for the channel wall fraction (e.g., 0.7).

The wave setup contribution to mean water level at the shoreline is calculated following Stockdon et al. (2006):

$$\eta_{setup} = 0.35 \beta_f \sqrt{H_0 L_0} \tag{7}$$

where β_f = beach foreshore slope; H_0 = deep-water wave height (m); L_0 = deep-water wavelength (m). Kraus and Hayashi 2005; Wamsley et al. (2006) discuss calculation of channel infilling and shoaling due to longshore transport estimates calculated from wave input data. Longshore transport is implemented in the coastal breaching model with the CERC formula in the *Coastal Engineering Manual* (Headquarters, U.S. Army Corps of Engineers 2002):

$$Q_l = K\left(\frac{\rho\sqrt{g}}{16\kappa^{\frac{1}{2}}\left(\rho_s-\rho\right)\left(1-n\right)}\right)H_{b\ rms}^{\frac{5}{2}}\sin\left(2\alpha_b\right) \tag{8}$$

where K = dimensionless sediment transport coefficient based on wave energy, κ=breaker index (non-dimensional ~ 0.8), n = sediment porosity, $H_{b\ \mathrm{rms}}$ = root-mean-square wave height at breaking point (m), and α_b = wave breaking angle.

The present study extends the capabilities of the morphologic breaching model by implementing multiple breaches with variable (in time and space) breach forcing. Furthermore, breaching model connectivity with the Cascade model is now possible by employing a subset of the wave and water surface elevation data used as inputs to Cascade, and spatially and temporally variable longshore sediment transport. Cascade output can control breach infilling and shoaling rates by longshore transport in place of Eq. 8 in the breaching model, subject of a planned future paper.

METHOD

An idealized alongshore barrier dune-crest topography (Fig. 1) was developed to simulate breaching at topographic lows in the dunes. This topography can be arbitrary, and the topographic lows function as potential pilot channels for the breaching model. Pilot channels of different elevations may exist, providing selective inundation for different water levels at various times in a storm and thereafter. Morphologic evolution of breach channels occurs only if the pilot channel is inundated. Local forcing, including longshore transport, waves, water level, and shoreline position for the breaches is provided at regional scale by the Cascade model. Sensitivity tests are conducted to isolate some of the complex processes that force change in breach morphology and to evaluate the functionality of the model under hypothetical forcing.

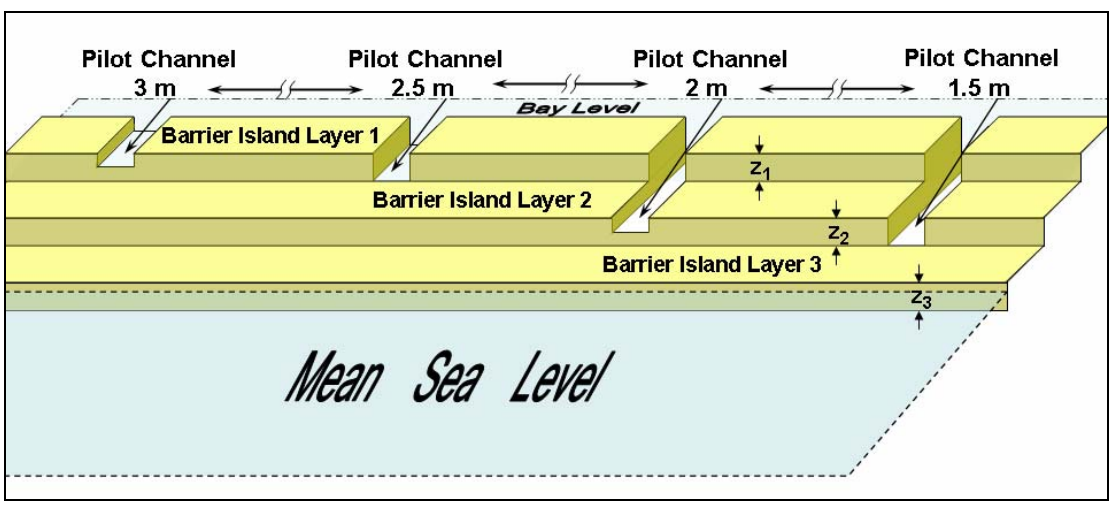

Fig. 1. Schematic of regional breaching model grid (vertically exaggerated)

Eight 14-day simulations of the evolution of multiple breach channels were conducted (Table 1) with the idealized barrier alongshore topography. Dune crest elevation was 3.5 m, and four different pilot channels 10 m wide by 50 m long were cut with elevations of 3, 2.5, 2, and 1.5 m. The location of the pilot channels along the barrier island is arbitrary and influenced only where input forcing is (optionally) extracted from Cascade. It is assumed that the breaches cannot converge, and therefore, pilot channels cannot be located at points along the barrier where the potential exists for two or more breaches to merge into one. Bay surface area was held constant at 5×10^8 m^2. The time-step for the simulations was set at 10 s. Empirical coefficients for sediment transport along the bottom and along the side of the breach were set to 0.5 and 0.7, respectively. Sediment porosity was 0.4, and the *K*-coefficient of the CERC formula was set to 0.39 (based on significant wave height). Finally, water (sediment) density was set to 1,025 kg/m^3 (2,650 kg/m^3).

The first sensitivity test (Case HD) held a constant 0.2-m head difference along the entire length of the barrier generated by a constant ocean water surface elevation at 3-m above MSL and a constant bay water surface elevation at 2.8-m above MSL. Two other cases were conducted employing the same constant head difference water level forcing between ocean and bay, added wave forcing to simulate wave setup forcing and sediment infilling due to longshore transport. Case HD-H1_T8_D0 includes waves with constant $H_0 = 1$ m, $T_0 = 8$ s, and $\alpha_0 = 0$ deg, and Case HD-H1_T8_D30 includes waves with constant $H_0 = 1$ m, $T_0 = 8$ s, and $\alpha_0 = 30$ deg.

Three sensitivity tests were conducted forced with a 1-m amplitude M_2 (12.42-hr period) tidal wave with 90-deg phase lag between the ocean and bay levels, applied along the entire length of the barrier with a vertical datum shift of 2-m above MSL. These cases are listed in Table 1 as Case M2, Case M2-H1_T8_D0, and Case M2-H1_T8_D30. Two cases also included wave forcing to estimate wave setup and sediment infilling due to longshore transport. Case M2-H1_T8_D0 includes waves with constant $H_0 = 1$ m, $T_0 = 8$ s, and $\alpha_0 = 0$ deg, and Case M2-H1_T8_D30 includes waves with constant $H_0 = 1$ m, $T_0 = 8$ s, and $\alpha_0 = 30$ deg.

The two remaining sensitivity tests examined response of the model to a synthetic storm surge. The first of the storm surge simulations (Case Surge in Table 1) was forced with a constant water level 1 m above MSL until day 5, after which a 2 m simulated parabolic storm surge extending over 2 days was added to initiate breach inundation (Fig. 2). This surge was set out of phase for each breach channel so that each breach would be initiated 6 hr after the previous breach. The second surge case (Case Surge+M2 in Table 1) consisted of the same synthetic surge as Case Surge, but the surge arrival was equal for all breaches, and a simple 1-m M_2 tide with 90-deg phase lag between the ocean and bay levels was added to the surge (Fig. 3). This M_2 tide differed from Case M2 in that it did not reach 2 m above MSL to prevent breach inundation prior to the surge arrival.

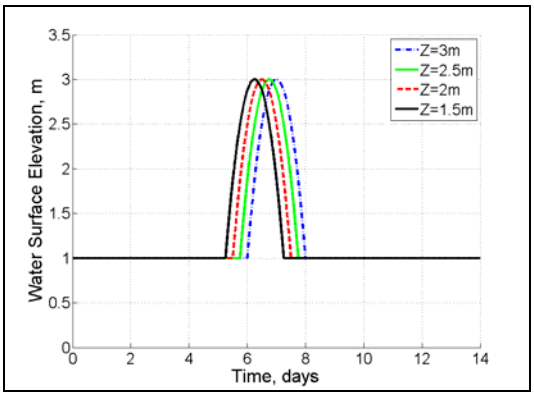

Fig. 2. Ocean and bay water level – Case Surge

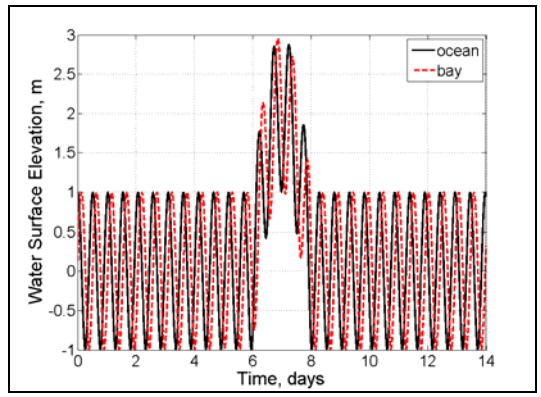

Fig. 3. Ocean and bay water level – Case Surge+M2

Table 1. Regional Breach Model Sensitivity Test Cases

Case Name	Water level forcing	Deep Water Wave Height (H_0), m	Deep Water Wave Period (T_0), s	Deep Water Wave Deg (α_0), deg
HD	Constant ocean = 3 m constant bay = 2.8 m	N/A	N/A	N/A
HD-H1_T8_D0	Constant ocean = 3 m constant bay = 2.8 m	1	8	0
HD-H1_T8_D30	Constant ocean = 3 m constant bay = 2.8 m	1	8	30
M2	M_2-tide amp: 1 m phase: ocean = 0° phase: bay = 90°	N/A	N/A	N/A
M2-H1_T8_D0	M_2-tide amp: 1 m phase: ocean = 0° phase: bay = 90°	1	8	0
M2-H1_T8_D30	M_2-tide amp: 1 m phase: ocean = 0° phase: bay = 90°	1	8	30
Surge	2-m storm surge w/6-min arrival delay for consecutive breach	N/A	N/A	N/A
Surge+M2	2-m storm surge + M_2-tide amp: 1-m phase:ocean = 0° phase: bay = 90°	N/A	N/A	N/A

RESULTS

Calculated evolution of breach channel depth, width, total transport through the four breaches, and cross-sectional area are shown in Figs. 4-7. Breaches that started in pilot channels at lower elevation (e.g., elevation $z = 1.5$ m, $z = 2$ m) were cut deeper (Fig. 4) and at a faster rate than those that developed in pilot channels at higher elevations (e.g., $z = 2.5$ m, $z = 3$ m). Conversely, the lateral growth of higher elevation channels in Fig. 5 is greater than the deeper, low-elevation channels. The greater lateral growth is explained by increased shear stresses by bottom friction in the sediment transport and hydrodynamic models. Breaching is not induced at the pilot channel stating at $z = 3$ m, because this elevation is the same as the ocean water surface elevation. Stair-shaped behavior observed in Fig. 6 is an artifact of the layered pyramidal barrier island, corresponding to the transport rates being reduced as a result of channel cuts into incrementally longer (in cross-shore orientation) barrier island layers. As breach channel depth increases, the transport can increase in magnitude and duration.

Figure 7 shows the breach cross-sectional area over the simulation period for Case HD. Breach channel cross-sectional area is a representation of the channel dimensions and serves as a good indicator of channel stability and channel evolution morphology. A delayed and extended incipient breaching stage occurs in the breach channel initially at $z = 2.5$ m relative to the channels at $z = 2$ and $z = 1.5$ m. This is, again, explained by the increased shear stress associated with shallow water over the channel bottom. A shallower channel is forced to grow laterally if sediment transport rates (Fig. 6) increase due to greater shear stress applied over a larger channel bottom surface area than generated in deeper breach channels.

Figures 8 and 9 compare breach channel cross-sectional area for Cases HD-H1_T8_D0 and HD-H1_T8_D30, respectively. Figure 8 retains many of the same patterns observed in the cross-sectional area plots of Case HD (Fig. 7). However, because of the presence of waves and the associated wave setup, a shorter incipient breaching stage is observed at the breach of $z = 2.5$ m, and the channel cross-sectional area for each breach in Fig. 8 at the end of the simulation is greater than those observed in Fig. 7. Figure 9 shows an entirely different pattern. In fact, due to the large incident wave angle relative to shoreline, significant longshore transport causes most of the channels to shoal. Breach closure does not occur for the breach at $z = 1.5$ m because this breach pilot channel is sufficiently deep to avoid closure during the incipient phase of the breach.

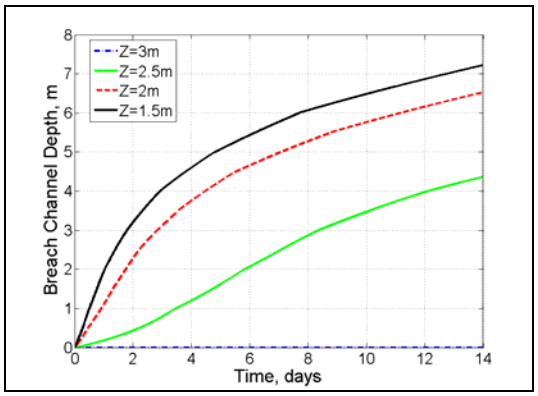

Fig. 4. Calculated breach depth , Case HD

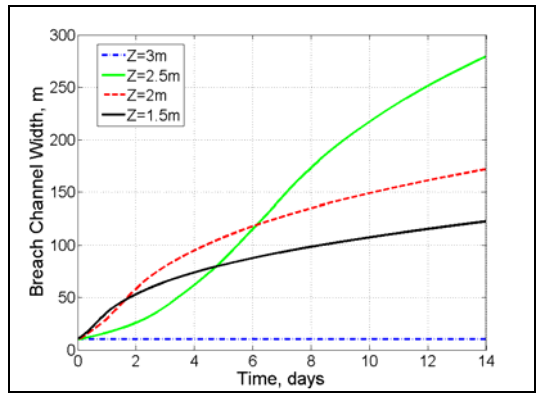

Fig. 5. Calculated breach width, Case HD

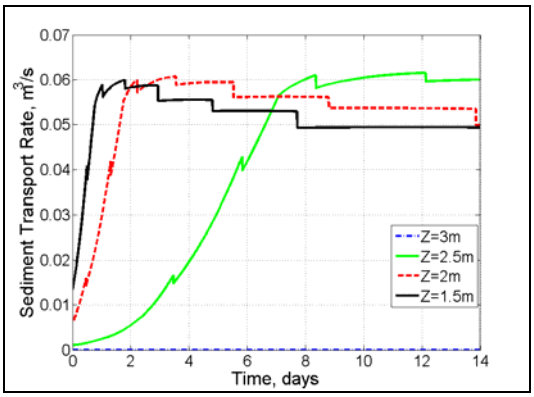

Fig. 6. Calculated sediment transport rate through the four breaches, Case HD

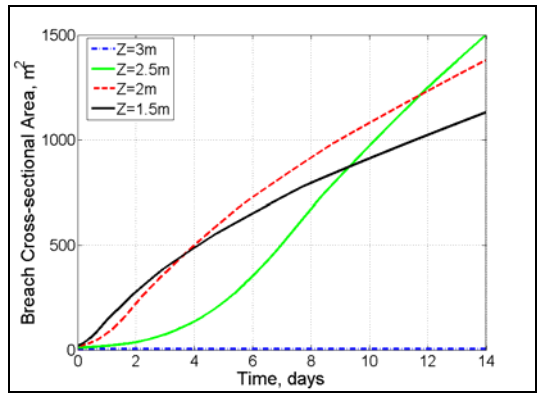

Fig. 7. Calculated Breach channel cross-sectional area evolution, Case HD

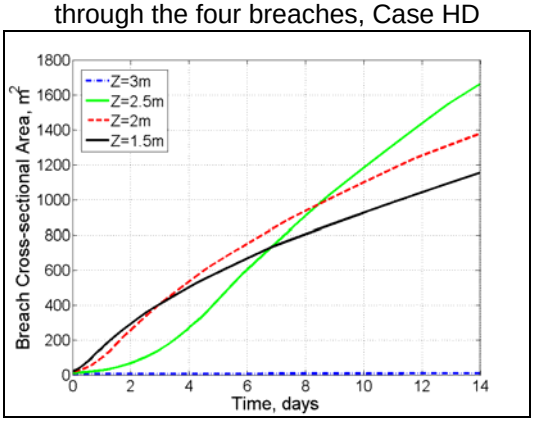

Fig. 8. Calculated Breach channel cross-sectional area evolution, HD_H1_T8_D0

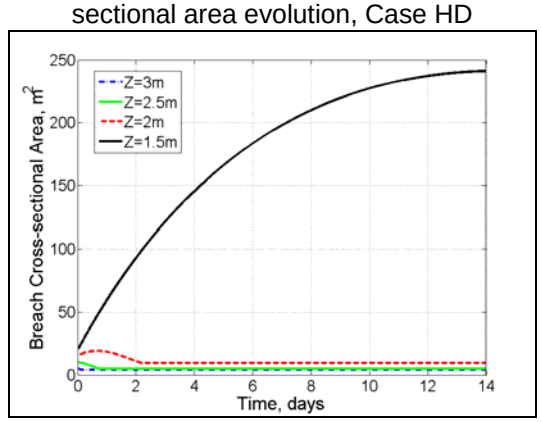

Fig. 9. Calculated Breach channel cross-sectional area evolution, HD_H1_T8_D30

Figures 10-13 illustrate breach transport and cross-sectional area for the M2, M2-H1_T8_D0, and M2-H1_T8_D30 cases. Figure 10 demonstrates the periodicity of sediment transport associated with the M_2 water elevation forcing. Depending on level of the breach channel relative to the forcing water level, transport rates may never approach zero, whereas sometimes the breach channel may be completely depleted of water as seen in Fig. 10 (z = 2.5 m). This switching on and off of transport rates

significantly reduces total transport through the breach as shown by the relative difference in cross-sectional area plots (Fig. 11) between $z = 2.5$ m and the much greater cross-sectional area represented in the $z = 1.5$ m and $z = 2$ m pilot channels. Case M2-H1_T8_D0 (Fig. 12) also demonstrates similar morphologic response as Case M2 (Fig. 11), but with slightly greater cross-sectional area and shorter incipient breach phase times. It appears that, in this case, the addition of wave setup has increased flow through the breaches, thereby increasing the channel area. Significant differences in cross-sectional area are achieved in Case M2-H1_T8_D30 with waves approaching at an incident angle (Fig. 13). This case suggests that breach channels can be overwhelmed by longshore sediment transport, and infilling occurs to the point of breach closure where breach evolution is constant, and the channels are no longer inundated.

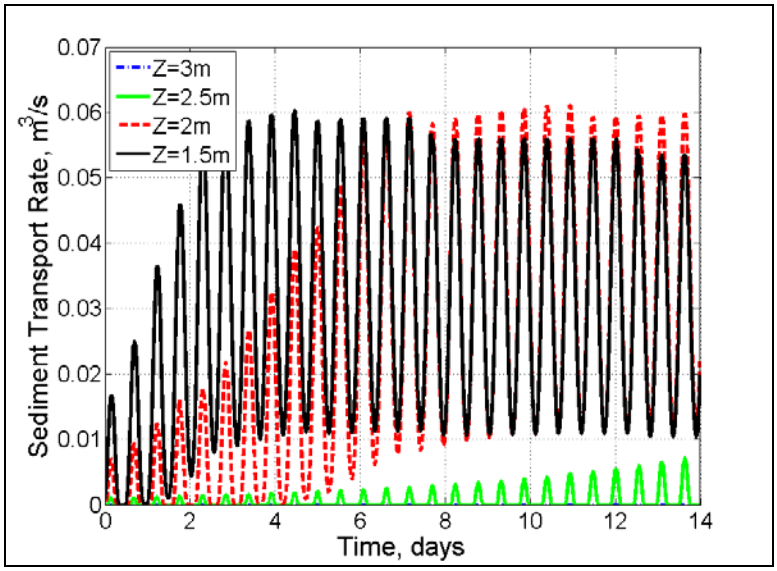

Fig. 10. Calculated sediment transport rate through the four breaches, Case M2

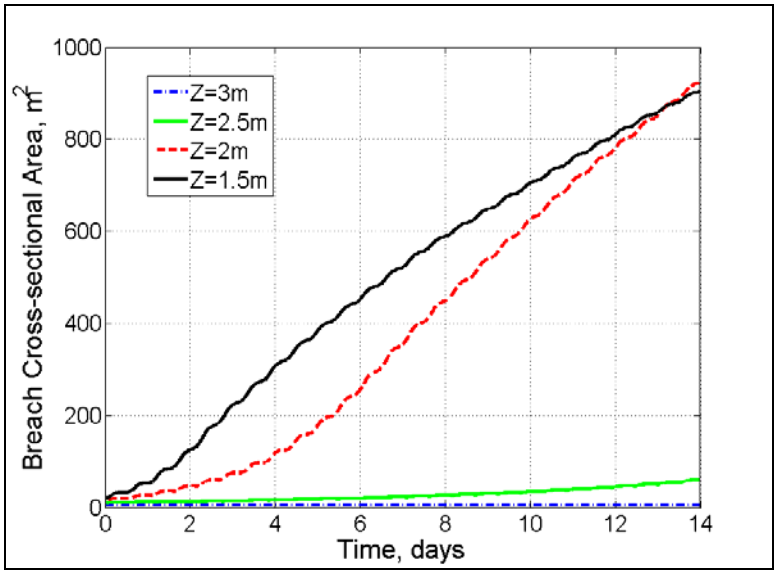

Fig. 11. Calculated breach channel cross-sectional area evolution, Case M2

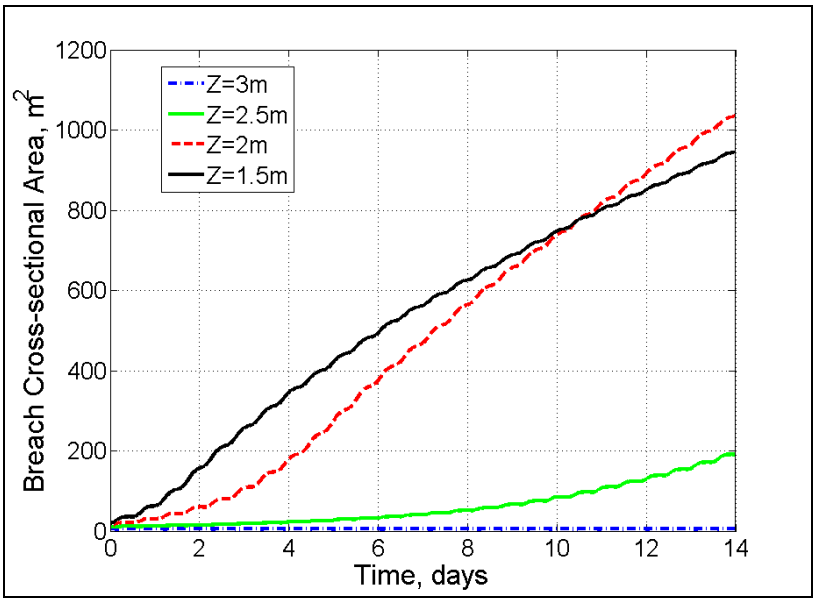

Fig. 12. Breach channel cross-sectional area evolution, Case M2-H1_T8_D0

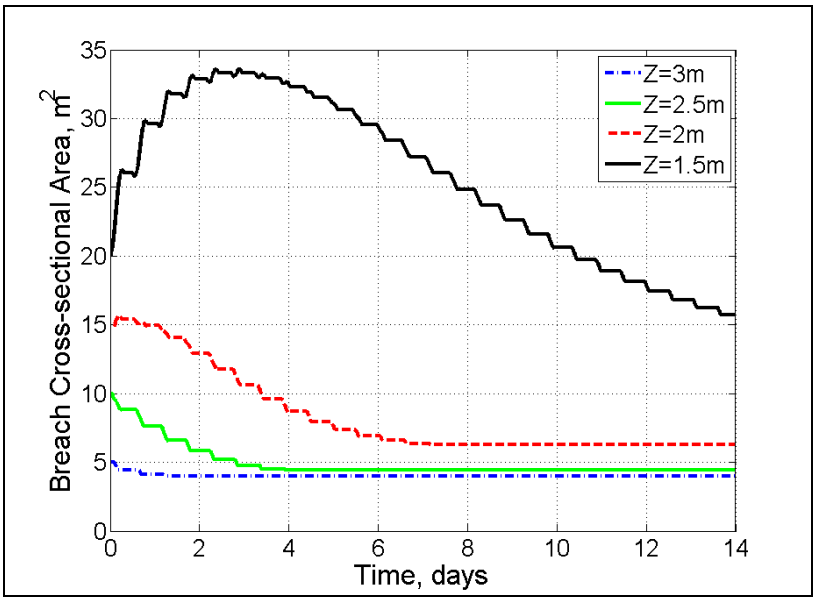

Fig. 13. Breach channel cross-sectional area evolution, Case M2-H1_T8_D30

Figures 14-17 illustrate breach transport and cross-sectional area for the Surge and the Surge+M2 cases. Because of the rapid increase in water level from the simulated storm surge, peaks in sediment transport (Fig. 14) are present immediately after inundation. These peaks grow progressively as pilot channels of initial elevations z = 1.5 m, z = 2 m, and z = 2.5 m are separately inundated and expanded. The growth of the peaks corresponds to the increase in incipient transport according to the depth of water in the breach channel. Shallow channels can transport more sediment because of larger bottom shear stress. Figure 15 indicates a rapid increase in cross-sectional area associated with the time of the storm surge.

Figure 16 illustrates the difference caused by addition of a tide to the storm surge. Because of the higher frequency M_2 tide relative to the surge, sediment transport (Fig. 16) goes to zero at periods of low tide during the surge. After the surge, transport rates for breaches at $z = 1.5$ m and $z = 2$ m continue to oscillate at the tidal frequency, indicating an open breach remains. Intermittent drying of the inlet causes a much reduced transport for the breach channels that had high pilot channels ($z = 3$ m, $z = 2.5$ m) where little to no inundation is present. Because of the reduced transport, the higher elevation channels remain closed after the surge, and cross-sectional area is constant (Fig. 17).

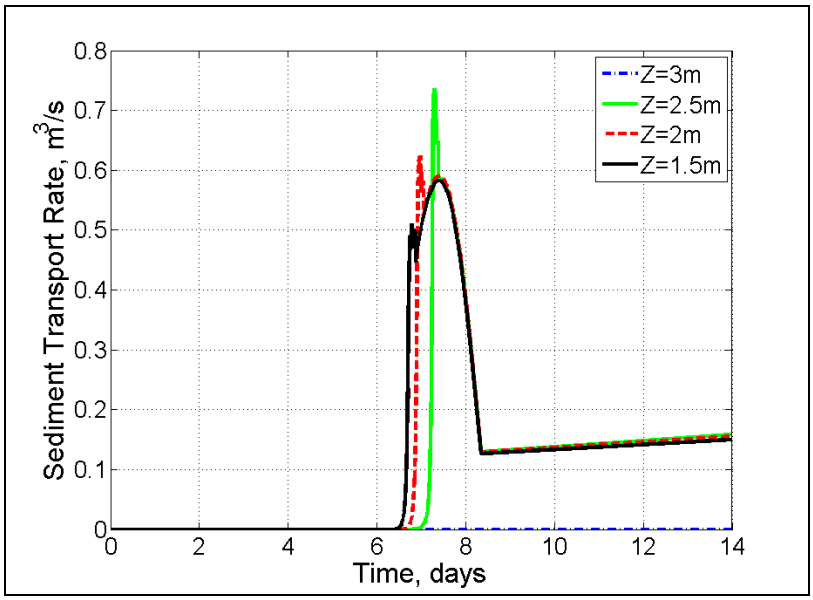

Fig. 14. Calculated sediment transport rate through the four breaches, Case Surge

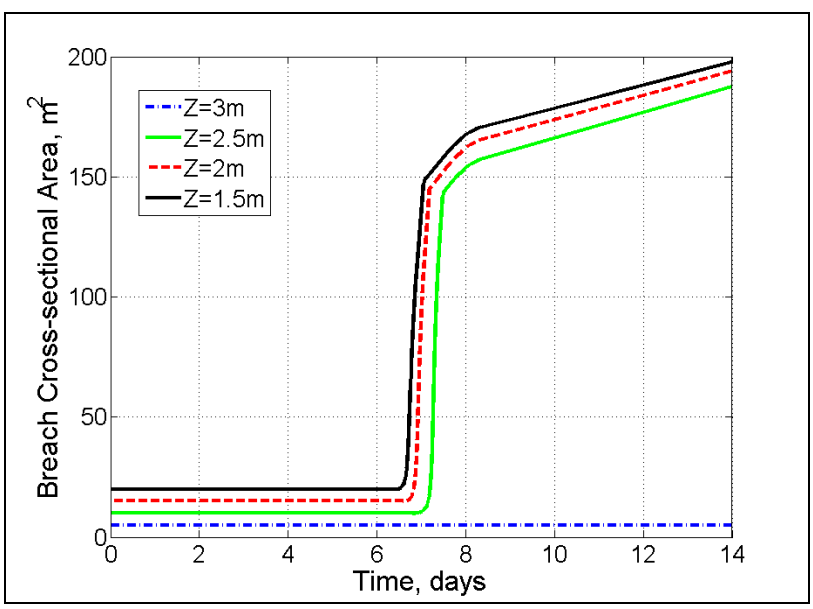

Fig. 15. Breach channel cross-sectional area evolution , Case Surge

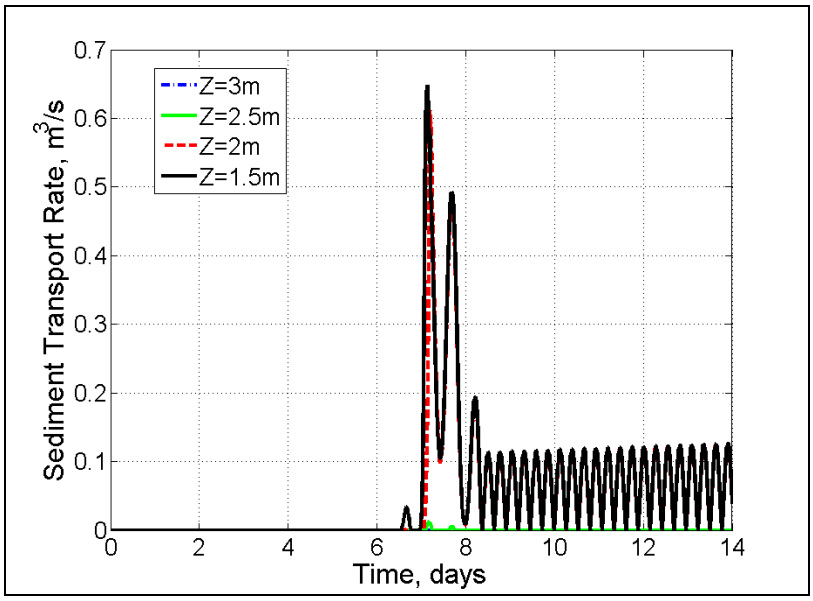

Fig. 16. Calculated sediment transport rate through the four breaches, Case Surge+M2

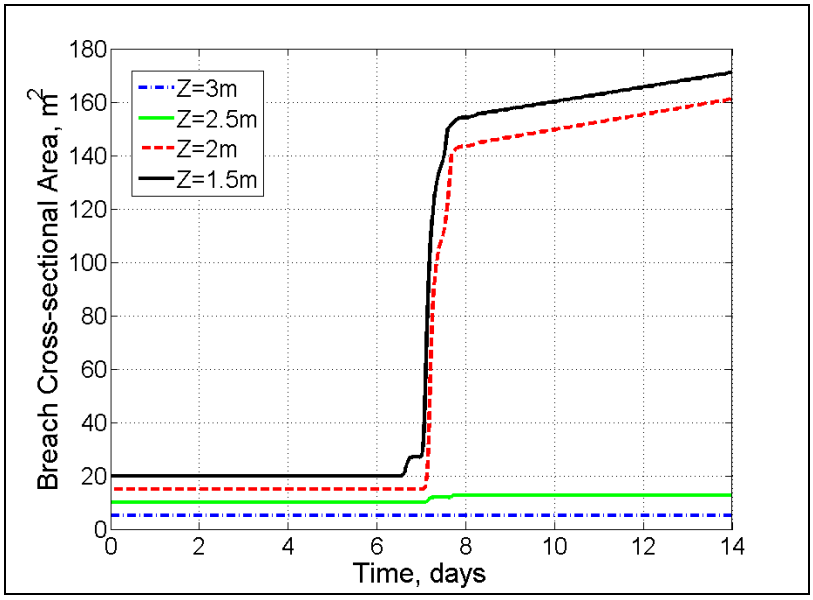

Fig. 17. Breach channel cross-sectional area evolution , Case Surge+M2

CONCLUDING DISCUSSION

This study investigated predictions of a new numerical model of multiple coastal barrier breaches at a regional scale allowing, for example, investigation of processes associated with independent evolution of each breach. Numerical simulations of coastal breaches at regional scale improve understanding of the physical processes by isolating forcing mechanisms and comparing responses of breach channels of varying dimensions. Enhancements to the morphologic breaching model add the capability to simulate multiple breach development at the regional scale with boundary condition forcing interaction with Cascade.

Calculation results indicate that slow, shallow inundation of breach pilot channels tends to produce breach width expanding at a greater rate than breach depth. This is likely due to the increased shear stress applied over a wider breach channel surface area in the model. A shallow breach also promotes a longer incipient breach phase and longer time before developing a tidally efficient channel. Fast and large inundation appears to promote rapid increase in depth as well as a more rapid incipient breach phase, where the cross-sectional area quickly changes.

Future research will examine model performance by comparison of predictions with observations of multiple breaches serving the same bay. Developments of the regional breaching model are expected to continue with an embedded form in Cascade for fully automated forcing and interaction. Finally, interaction between breaches serving the same bay will need to be represented for examining multiple inlet stability for a nearly fixed available tidal prism.

ACKNOWLEDGEMENTS

This study was conducted as an activity of the Coastal Morphology Modeling and Management (Cascade) work unit of the System-Wide Water Resources Program (SWWRP) with support from the Coastal Inlets Research Program (CIRP) conducted at the U.S. Army Engineer Research and Development Center. Permission was granted by Headquarters, U.S. Army Corps of Engineers, to publish this information.

REFERENCES

Connell, K.J., and Kraus, N.C. (2006). "Cascade Version 1: User's guide," ERDC TNSWWRP-06-5, U.S. Army Engineer Research and Development Center, Vicksburg, MS, (https://swwrp.usace.army.mil/).

Freeman, C.W., Bernstein, D.J., and Mitasova, H. (2004). "Rapid response 3D survey techniques for seamless topo/bathy modeling: 2003 Hatteras Breach, North Carolina," *Shore & Beach* 72(2), 3-7.

Hayes, M.O. (1967). "Hurricanes as geological agents, south Texas coast," *American Assoc. Petroleum Geologists Bull.* 51, 937-942.

Headquarters, U.S. Army Corps of Engineers. (2002). *Coastal Engineering Manual*, EM 1110-2-1100, Washington, DC.

Keulegan, G.H. (1967). "Tidal flow in entrances: Water level fluctuations of basins in communication with the seas," Committee on Tidal Hydraulics Technical Bulletin No. 14, U.S. Army Engineer Waterways Experiment Station, Vicksburg, MS.

Komar, P.D. (1998). "*Beach processes and sedimentation*," 2nd edition, Prentice-Hall, NJ, 544 p.

Kraus, N.C. (1998). "Inlet cross-sectional area calculated by process-based model," *Proc. 29th Coastal Eng. Conf*, ASCE, 3,265- 3,278.

Kraus, N.C. (2003). "Analytical model of incipient breaching of coastal barriers," *Coastal Eng. Journal*, 45(4), 511-531.

Kraus, N.C., and Hayashi, K. (2005). "Numerical morphological model of barrier island breaching," *Proc. 29th Coastal Eng. Conf.*, World Scientific Press, 2,120-2,132.

Kraus, N.C., and Wamsley, T.V. (2003). "Coastal barrier breaching. Part 1: Overview of breaching processes," Coastal and Hydraulics Laboratory Technical Note ERDC/CHL CHETN IV-56, U.S. Army Engineer Research and Development Center, Vicksburg, MS, (http://chl.wes.army.mil/library/publications/chetn).

Larson, M., and Kraus, N.C. (2003). "Modeling regional sediment transport and coastal evolution along the Delmarva Peninsula, USA," *Proc. Coastal Sediments '03*, World Sci. Press., CD-ROM, East Meets West Productions, ISBN-981-238-422-7, 14 p.

Larson, M., Kraus, N.C., and Hanson, H. (2003). "Simulation of regional longshore sediment transport and coastal evolution - the 'Cascade' model," *Proc. 28th Coastal Eng. Conf.*, World Sci. Press, 2,612-2,624.

Larson, M., Kraus, N.C. and Connell, K.J. (2006). "Cascade Version 1: Theory and model formulation," ERDC TN-SWWRP-06-7, U.S. Army Engineer Research and Development Center, Vicksburg, MS, (https://swwrp.usace.army.mil/).

Larson, M., Kraus, N.C., Connell, K.J. (2007). "Modeling sediment storage and transfer in large-scale coastal evolution models," *Proc. 30th Coastal Eng. Conf.*, in press.

Price, W.A. (1947). "Equilibrium of form and forces in tidal basins of coast of Texas and Louisiana," *American Assoc. Petroleum Geologists Bull.* 31, 1,619-1,663.

Stockdon, H.F., Holman, R.A., Howd, P.A., and Sallenger, A. H. (2006). "Empirical parameterization of setup, swash, and runup," *Coastal Eng.* 53(7), 573-588.

Terchunian, A.V., and Merkert, C.L. (1995). "Little Pikes Inlet, Westhampton, New York," *J. Coastal Research* 11(3), 697-703.

Wamsley, T.V., and Hathaway, K.K. (2004). "Monitoring morphology and currents at the Hatteras Breach," *Shore & Beach* 72(2), 9-14.

Wamsley, T.V., and Kraus, N.C. (2005). "Coastal barrier island breaching, Part 2: Mechanical breaching and breach closure," Coastal and Hydraulic Laboratory Technical Note ERDC/CHL CHETN IV-65, U.S. Army Engineer Research and Development Center, Vicksburg, MS, 21 p, (http://chl.wes.army.mil/ library/ publications/chetn).

Wamsley,T.V., Kraus, N.C., Larson, M., Hanson, H., Connell, K.J. (2007). "Coastal barrier breaching: Comparison of numerical and physical models," *Proc. 30th Coastal Eng. Conf.*, World Sci. Press, in press.

Wamsley, T.V., Cialone, M.A., Connell, K.J., Kraus, N.C. (2006). "Breach history and susceptibility study, south jetty and navigation project, Grays Harbor, Washington," Coastal and Hydraulics Laboratory Technical Report ERDC/CHL TR-04-2, U.S. U.S. Army Engineer Research and Development Center, Vicksburg, MS.

Watanabe, A., Shimuzu, T., and Kondo, K. (1991). "Field application of a numerical model of beach topography response," *Proc. Coastal Sediments '91*, ASCE Press, 1,814-1,928.

Wutkowski, M. (2004). "Hatteras Breach closure," *Shore & Beach* 72(2), 20 -24.